Bull Volcanol (2007) 69: 353–363
DOI 10.1007/s00445-006-0080-7

RESEARCH ARTICLE

Emily K. Desmarais · Paul Segall

Transient deformation following the 30 January 1997 dike intrusion at Kīlauea volcano, Hawai'i

Received: 3 June 2005 / Accepted: 5 April 2006 / Published online: 29 June 2006

Abstract On 30 January 1997 an intrusion on Kīlauea volcano opened a new fissure within the East Rift Zone (ERZ) at Nāpau Crater, 3 km uprift from the ongoing eruptions at Pu'u 'Ō'ō. The fissure eruption lasted 22 h and opened a 5.1 km long, nearly vertical dike 1.9 m, extending from the surface to a depth of 2.4 km (Owen et al. 2000b). During the eruption, the lava pond at Pu'u 'Ō'ō drained, and eruptions ceased there. Pu'u 'Ō'ō eventually refilled in late February and eruptions resumed there on 28 March 1997. Continuous GPS data show a large transient following the 30 January 1997 dike intrusion. After lengthening 40 cm during the initial eruption, the baseline between two stations spanning the ERZ lengthened an additional 10 cm over the following 6 months. A coastal station KAEP also exhibited transient deformation, as it continued to move southward (5 cm) over the same 6-month period. The baseline between two stations spanning Kīlauea's summit caldera contracted sharply during the eruption, but gradually recovered to slightly longer than its previous length 2 months after the intrusion. We use the extended network inversion filter (McGuire and Segall 2003) to invert continuous GPS data for volume change of a spherical pressure source under Kīlauea's summit, opening distribution on a nearly vertical dike in the ERZ and potential slip on a decollement 9 km beneath the south flank. Following the 30 January intrusion, rift extension continued below the initial dike intrusion for the duration of the transient. Decollement slip, regardless of its assumed depth, is not required to fit the data. The modeled transient summit reinflation and rift opening patterns under Nāpau crater coincide with changes in observed behavior of Pu'u 'Ō'ō's lava pond. Rift opening accelerated while Pu'u 'Ō'ō eruptions paused and began to decelerate after the lava pond reappeared nearly a month after the Nāpau eruption. The transient deformation is interpreted as resulting from shallow accommodation of the new dike volume.

Keywords Kīlauea · Transient · Deformation · Extended network inversion filter · Dike · Intrusion

Editorial responsibility M. Ripepe

E. K. Desmarais (✉) · P. Segall
Department of Geophysics,
397 Panama Mall,
Stanford, CA 94305, USA
e-mail: emilyd@stanford.edu
Tel.: +1-650-7239594
Fax: +1-650-7250979

Introduction

Deformations accompanying dike intrusions and fissure eruptions have been observed with a variety of geodetic techniques. These include: GPS, InSAR, tilt, trilateration, strain, and leveling (Owen et al. 2000a,b; Jónsson et al. 1999; Amelung et al. 2000; Okada and Yamamoto 1991; Bonaccorso and Davis 1993; Du and Aydin 1992). The short term, co-intrusive deformations are well modeled using elastic dislocation theory. There are numerous examples of co-intrusive modeling in the literature from Hawai'i, Iceland, Italy, Japan, the Galapagos and the Afar region of Africa (Owen et al. 2000b; Foulger et al. 1992; Bonaccorso et al. 2002; Okada and Yamamoto 1991; Jónsson et al. 1999; Amelung et al. 2000; Walpersdorf et al. 1999).

In addition to co-intrusive displacements, transient displacements have been observed in the weeks, months and years following large intrusive episodes. For example, Foulger et al. (1992) analyzed GPS data collected between 1987 and 1990 from Krafla volcano, Iceland and found that the time averaged ridge spreading rate could not account for all of the observed deformation. They attributed the excess deformation to viscoelastic relaxation of the asthenosphere following a series of about 20 rifting events that began in 1975 (Bjórnsson et al. 1977, 1979; Sigurdsson 1980). Alternatively, Thatcher (1992) questioned whether the same deformation pattern might be attributed to time-dependent opening deep within the rift zone.

Indeed, transient deformation following intrusions is to be expected. Typical basaltic dikes are meters thick and anywhere from one to hundreds of square kilometers in area. Stress changes associated with emplacement of such

dikes can result in time-dependent deformation of the surrounding crust as it accommodates the new volume.

Here we investigate the sources of time dependent deformation following a relatively small, but well-monitored eruption and intrusion into the East Rift Zone (ERZ) of Kīlauea volcano, Hawai'i in 1997. A small amount of magma was erupted at the surface, but the majority of it was intruded into the East Rift Zone (Owen et al. 2000b).

Kīlauea volcano

Kīlauea volcano (Fig. 1) is extremely active both magmatically and tectonically. Kīlauea volcano has been erupting more or less continuously since 1983 from the Pu'u 'Ō'ō and Kūpaianaha vents in the ERZ. Additionally, Kīlauea experiences large earthquakes, including the 1868 M8 Kau earthquake (Wyss 1988), the 1975 M7.2 Kalapana earthquake (Ando 1979) and the 1989 M6.1 South Flank earthquake (Árnadóttir et al. 1991; Hooper et al. 2002). The focal mechanisms of these events are characterized by one sub-horizontal nodal plane, with the upper plate moving southeast (Klein 1981).

It has been suggested that these earthquakes occur at the base of the volcanic pile on a decollement interpreted as the interface between the volcano and the Cretaceous sea floor (Nakamura 1980). However, the precise depth of the earthquakes is not well constrained (Klein et al. 1987; Thurber and Gripp 1988). Catalog locations of earthquakes on Kīlauea's south flank, the area south of the ERZ and the Southwest Rift Zone (SWRZ), show considerable scatter in focal depth, ranging from 5 to 13 km (Klein et al. 1987). Earthquake relocations using waveform cross-correlation techniques (Got et al. 1994; Got and Okubo 2003) improve the depth resolution and show that many of the south flank events collapse to a single surface. In a combined inversion, Hooper et al. (2002) model the 1989 M6.1 Kīlauea south flank earthquake using GPS, leveling and EDM data with relocated aftershocks and concluded that the earthquake depth is consistent with a decollement source.

General trends in deformation on Kīlauea can be characterized by inflation-deflation cycles of the summit region (Dvorak and Dzurisin 1997), extension across the ERZ, and gradual southward motion of the entire south flank (Dieterich 1988; Delaney et al. 1998; Owen et al. 2000a). These characteristics are all observed in the long-term velocities determined by GPS. Sites well north of the ERZ are relatively stable, while south central coastal sites displace seaward at rates as high as 8 cm/year, as estimated from GPS data collected between 1990 and 1996 (Owen et al 2000a). Owen et al. (2000a) show that the long term

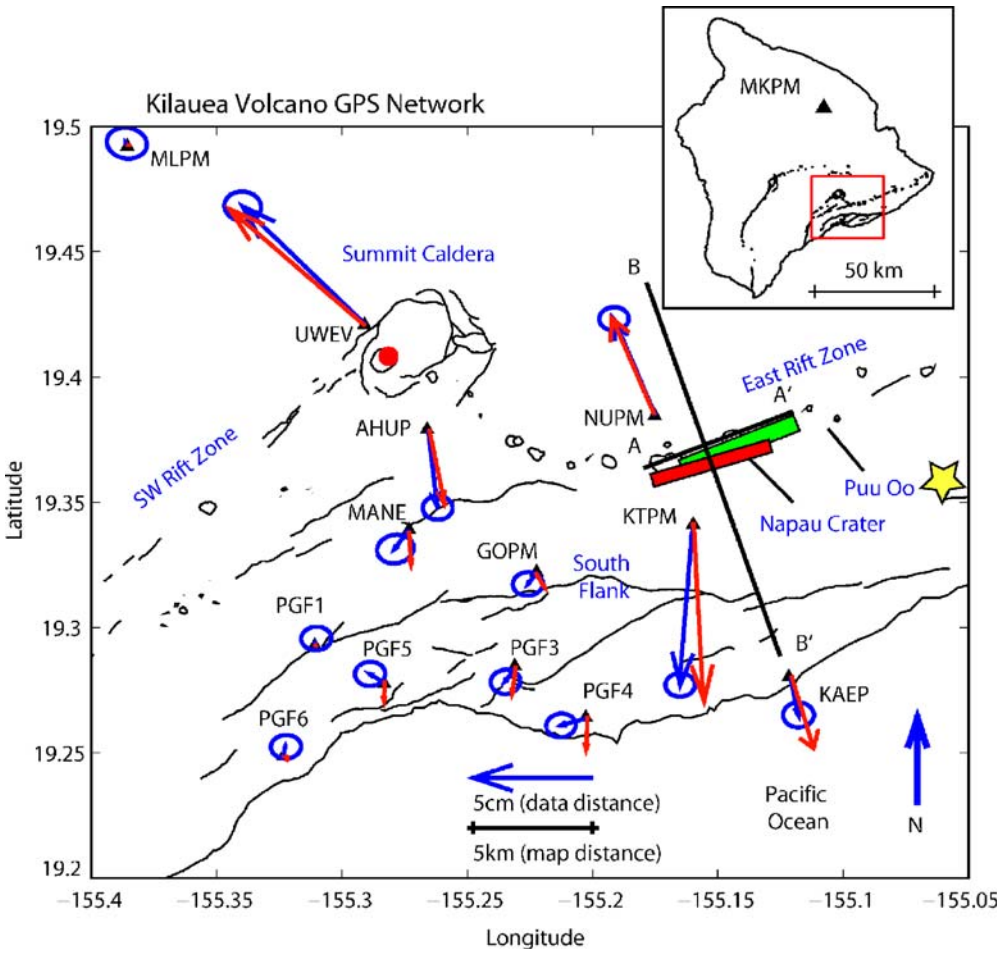

Fig. 1 Volcanic landmarks and continuous GPS stations on Kīlauea volcano, Hawai'i with cumulative post-intrusion transient displacements for the time period between 1 February 1997 and 31 December 1997. Error ellipses are 95% confidence intervals. The initial 30 January 1997 dike is shown in *green*. The best-fitting cumulative transient dike, and predicted displacements are shown in *red*. The epicenter of the M5.7 earthquake that occurred on 30 June 1997 is shown by the *yellow star*

deformation can be explained by combining deflation of the summit magma reservoir, 20–30 cm/year slip on the decollement and 20 cm/year opening in the deep ERZ, and 12 cm/year of strike slip in the upper ERZ.

30 January 1997 intrusion

Early on the morning of 30 January 1997 a new fissure opened within Nāpau crater, 3 km uprift of the Pu'u 'Ō'ō vent (Heliker et al. 1997). Eventually, a total of six fissures formed erupting a 300,000 m^3 mixture of relatively hot fresh basalt and cooler, fractionated, rift-stored basalt (Thornber et al. 2003). The Nāpau eruption lasted only 22 h in what is now known as Episode 54 of the Pu'u 'Ō'ō Kūpaianana eruption. Owen et al. (2000b) determined co-intrusive displacements from continuous and campaign GPS measurements before and after the intrusion. These displacements were best described by a nearly vertical, 5.15 km long dike with 1.96 m of opening, which extended from the surface to a depth of 2.4 km (Fig. 1). The dike intruded 20×10^6 m^3 of basalt into the shallow rift zone.

The intrusion was preceded by 8 h of volcanic tremor and accelerated extension of the ERZ (Owen et al. 2000b; Segall et al. 2001). During the eruption, the lava pond at Pu'u 'Ō'ō drained and a section of the cone collapsed (Thornber et al. 1997). It has been postulated that the beginning of tremor, which is related to subsurface fluid flow, coincided with the onset of dike propagation (Thornber et al. 1997). Following the short-lived Nāpau eruption, activity at Pu'u 'Ō'ō stopped for nearly a month; the lava pond refilled in late February and eruptions resumed 28 March 1997 (Owen et al. 2000b).

Kīlauea's summit caldera was slowly and steadily contracting at about 2 cm/year throughout late 1996 and did not show any change immediately prior to the 30 January 1997 eruption. During the intrusion the summit caldera-crossing baseline, AHUP-UWEV, rapidly shortened by 10 cm, indicating rapid deflation of the summit magma chamber (Fig. 2). Between the intrusion and the first week of April the magma chamber recharged. On 30 March 1997, the baseline AHUP-UWEV recovered its previous length 2 days after the resumption of the eruption at Pu'u 'Ō'ō (Owen et al. 2000b), indicating that pressure equilibrium was obtained between the summit and Pu'u 'Ō'ō (Segall et al. 2001).

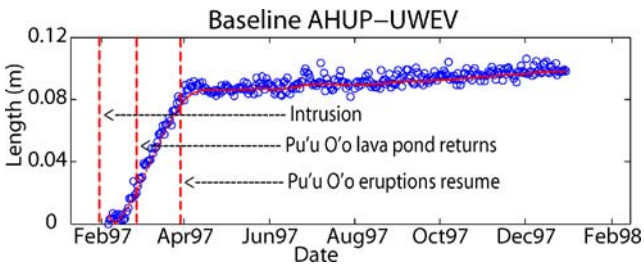

Fig. 2 Baseline length from AHUP to UWEV, which spans the summit crater. The time series begins just after the Nāpau eruption

The lack of pre-eruptive summit inflation and the fact that Pu'u 'Ō'ō provided an open vent for magma to exit the system suggests that the Nāpau dike injection could not have been driven by a pressure increase in the summit magma reservoir. Owen et al. (2000b) concluded that the dike intrusion was passive and that the rift failed in extension due to accumulated south flank motion. Cervelli et al. (2002b) also showed that the upper ERZ, in particular was subject to significant extensional stresses prior to the 30 January 1997 intrusion. The cumulative extension across this part of the rift from the beginning of the Pu'u 'Ō'ō eruption in 1983 to 1997 was roughly 2 m, which is equivalent to the estimated thickness of the 30 January 1997 dike.

Thornber et al. (2003) showed that the erupted magmas at Nāpau crater contained a substantial fraction of evolved magmas from the 1963 and 1968 Nāpau eruptions. This adds to earlier evidence that pockets of melt reside within the rift zone for extended periods of time. Thornber et al. (2003) suggest that these small isolated pockets of cooler magma which separated from the active rift zone conduit made Nāpau crater weaker and prone to failing in extension.

Data

The 12 continuous GPS sites analyzed in this paper are from the Kīlauea volcano GPS network, which is collaboratively operated by the Hawai'ian Volcano Observatory (HVO), Stanford University and the University of Hawai'i. The data span 1 February–31 December 1997 and have been differenced to the permanent GPS station, MKPM, on Mauna Kea, effectively removing the Pacific plate velocity. No models investigated here predict any discernible deformation at Mauna Kea.

The network began recording at UWEV and MANE in 1995; the remainder of the GPS stations were installed in 1996. Daily solutions are computed at the Hawai'ian Volcano Observatory using the GIPSY/OASIS II software package developed at JPL in precise point-positioning mode with non-fiducial orbits (Gregorius 1996; Zumberge et al. 1997). After processing, the daily non-fiducial solutions are transformed into a global ITRF2000 reference frame with a 7-parameter Helmert transformation provided by JPL (Cervelli et al. 2002b).

After the 30 January 1997 eruption, a decaying transient lasting several months was observed in the continuous GPS data localized around Nāpau crater and the summit caldera (Fig. 3). KTPM, to the south of the fissure, moved an additional 7 cm to the south and NUPM, to the north of the fissure, moved 3 cm towards the north, implying continued extension across the East Rift Zone. Vertical displacements at both NUPM and KTPM show uplift in the first month after the intrusion but, vertical displacements at other rift zone and flank sites were negligible. At the summit caldera spanning sites, AHUP and UWEV, large transients are seen in both in the horizontal and vertical components. AHUP and UWEV, moved radially outward from the summit caldera, consistent with reinflation of the summit magma chamber.

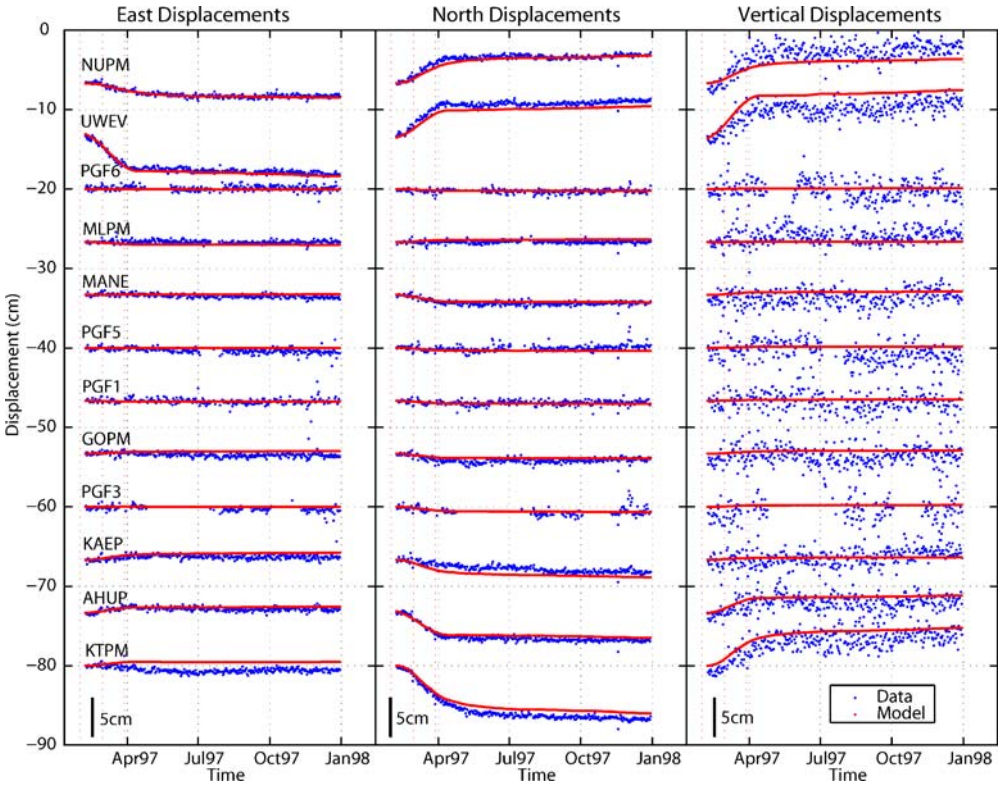

Fig. 3 East, north and vertical components of the Kīlauea GPS network showing transient signals following the 30 January 1997 intrusion. The data are in *blue* and the model predicted positions are in *red*. The data have been differenced to Mauna Kea and were detrended using estimates of average velocity from 3 years of data following the transient deformation. *Error bars* on the tightly constrained solutions are smaller than the size of the markers

In order to isolate the transient deformation observed from 1 February–31 December 1997, we removed secular velocities, $\mathbf{v}_{sec}$, from the time series prior to the time-dependent inversion. Removing secular velocities helps to simplify modeling by highlighting departures from quasi-steady state deformations. Average velocities were estimated by a least squares inversion of all available data following the transient from 1997.6 to 2003.0. We simultaneously estimated the three components of velocity at each station and the instantaneous offsets associated with small magmatic events and moderate sized earthquakes (Table 1). These average velocities of up to 6cm/year are most likely attributed to secular sliding on the decollement surface at a depth of about 10 km and some opening of the deep rift zone between 6–10 km (Owen et al. 2000b). In addition, we removed offsets of up to 1 cm at each site associated with a M5.2 earthquake which occurred in the eastern part of the network on 30 June 1997. The resulting cumulative post-intrusion transient displacements are shown in Fig. 1.

Method

We use the extended network inversion filter (ENIF; McGuire and Segall 2003; Miyazaki et al. 2003) to invert for the time-dependent sources of transient deformation following the 30 January 1997 ERZ intrusion. The ENIF is an extension of the network inversion filter (NIF; Segall and Matthews 1997) which employs a Kalman filter for combining observations with a priori information about the physical or stochastic nature of a system.

At each time step, the Kalman filter first makes a prediction of the next observation based on the model and a priori information. The prediction is then compared with the next observation and the model is updated. The filter progresses through this cycle of prediction-update operations until the end of the data set. Rather than assuming a specific functional form (i.e., exponential or logarithmic) of the fault slip or dike opening history, the NIF uses a stochastic integrated random walk model for the temporal evolution of deformation (Segall and Matthews 1997;

Table 1 Known tectonic and magmatic events during the time span used to estimate steady-state velocity (January 1997–January 2001)

Event	Date	Reference
Nāpau crater (Episode 54) eruption/intrusion	30 January 1997	Owen et al. (2000b)
M5.2 south flank earthquake	30 June 1997	Owen et al. (1997)
Summit tilt event	14 January 1998	Larson et al. (2001)
Slow earthquake	19 September 1998	Desmarais et al. (2005)
M5.6 Pahala earthquake	12 September 1999	Cervelli et al. (2002a)
Poliokeawe Pali earthquake swarm	21 November 1999	None
Slow earthquake	10 November 2000	Cervelli et al. (2002b)

Miyazaki et al. 2003). Simultaneous network inversion within the NIF, rather than looking separately at individual time series, enables the filter to separate spatially coherent deformation signals from spatially incoherent local noise, both of which may be time-varying.

Cumulative static model

We estimated the source geometry from the transient displacements accumulated following the intrusion and found the best fitting source to be a planar body just below the initial dike intrusion. The summit magma chamber is modeled as a point source of volume change at a depth of 1.2 km (Owen et al. 2000b) in an elastic half space (Mogi 1958). The dike and decollement were modeled as uniform elastic dislocations in a half space (e.g., Okada 1985). The half-space solutions are reasonably accurate on shield volcanoes like Kīlauea because of their shallowly sloping flanks, but do not address variable elastic rock properties. The half-space surface is defined by the best-fitting horizontal plane through the GPS stations, and is the same reference for the rift zone and summit. Slip was also estimated on a decollement at depths allowed to vary between 3 and 15 km.

We used simulated annealing (Metropolis et al. 1953; Creutz 1984) to solve for the optimal source geometry by minimizing the misfit between the cumulative observed transient deformation and predicted deformation. The cumulative displacements used to optimize the post-intrusion transient source geometry were from 1 February 1997 to 31 December 1997. The best fitting dike orientation and position are then held fixed for the time-dependent inversion.

The optimal model to fit the cumulative static data includes a uniform opening dike and no decollement. The dike is 5.3 km long and 2.7 km wide with the bottom at a depth of 4.5 km , and 0.08 m of opening (Fig. 5). There is no apparent shear across the rift zone. The optimal strike (70°) and dip (84°) are similar to the eruption model of (Owen et al. 2000b), but the center of the best-fitting transient deformation geometry is located 1.1 km west and 2 km deeper than the center of the initial eruption model as estimated by Owen et al. (2000b). The post-eruption opening is just below the co-eruptive dike.

Because we are primarily concerned with the time dependence of the transient opening, and the time history is not affected by small changes in the location of the transient dike, we only present a qualitative assessment of the bounds on each parameter. As opposed to the co-intrusive dike inversion done by Owen et al. (2000b), which used several campaign sites in addition to the continuous sites to determine the dike geometry, we have only twelve continuous sites, making the problem much less well defined. Only two continuous sites are close to the dike, NUPM and KTPM, thus we do not have particularly good resolution along the strike to determine the length of the transient intrusion. Depth and width, as discussed in the next section, are well enough resolved to differentiate a shallow (0–2 km deep) opening from a 2–4 km opening. The dip is also not well resolved, but is consistently within

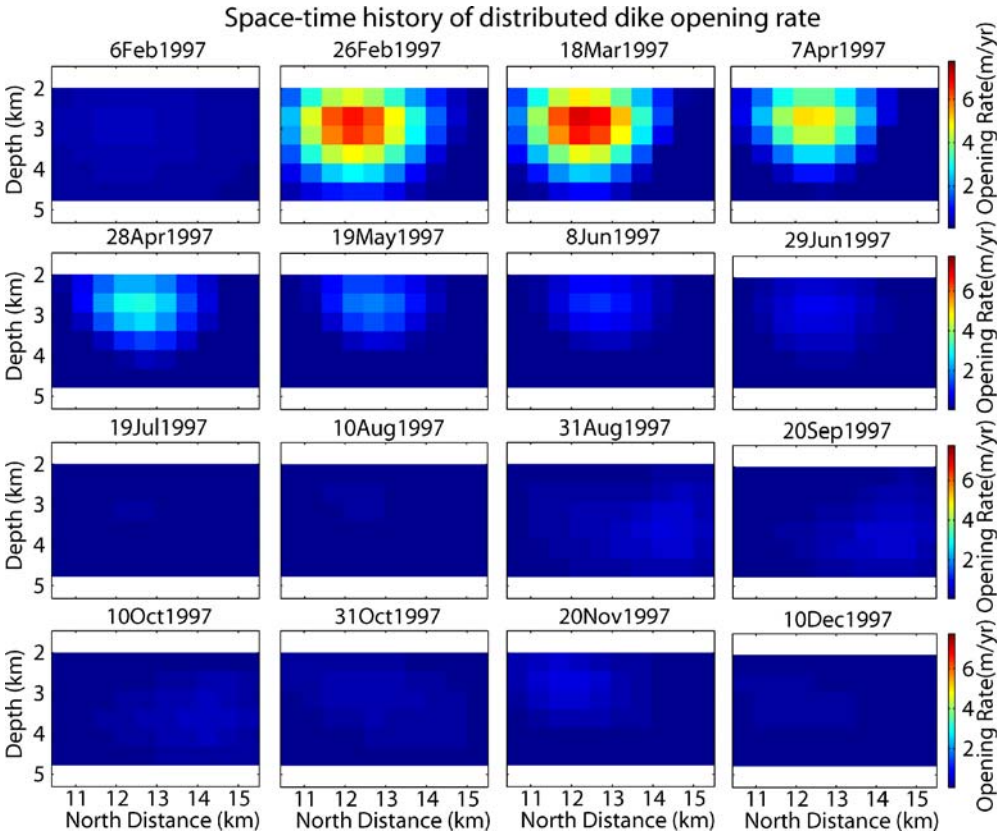

Fig. 4 Space–time history of distributed dike opening rate following the 30 January 1997 dike intrusion. This figure is read like a filmstrip starting in the *upper left corner*. *Warm colors* indicate opening

of 5–7° of vertical. This range of dips is observed in the exposed rift zone of Ko'olau (Walker 1987). Strike and position are primarily defined by the rift zone geology.

Time and space dependent model

We model the post-intrusion deformation as resulting from a combination of transient rift opening, $P(t)_{\text{rift}}$, transient decollement slip, $S(t)_{\text{decollement}}$ and volume change of the summit magma chamber, $V(t)_{\text{mogi}}$. In practice, we only estimate rift opening and magma chamber volume since including the decollement does not significantly improve the solution.

In addition to deformation signals, the GPS data include various sources of noise including random benchmark motions, $L(x,t—t_o)$, modeled as Gaussian random walk. ε represents unmodeled white noise errors, including multi-path, unmodeled atmospheric phase delays, and all other sources of unmodeled error. A Helmert transformation, $F\mathbf{f}(t)$, accounts for rigid translations, rotations, and scaling due to daily errors in realizing a stable GPS reference frame. Here, f(t) is assumed to be a white noise process (i.e., uncorrelated in time). Thus, the observation equation we use is:

$$\begin{aligned}\Delta\mathbf{X} - \mathbf{v}_{\text{sec}}t \\ = G\mathbf{m}(\mathbf{t}) + L(\mathbf{x}, t - t_{\text{o}}) + F\mathbf{f}(t) + \boldsymbol{\varepsilon}\end{aligned} \tag{1}$$

where $\Delta X—\ v_{\text{sec}}t$ is the position of the GPS antenna, relative to an a priori estimate, and corrected for average velocity, $\mathbf{v}_{\text{sec}}t$. G are the elastic Green's functions in a homogeneous isotropic half-space which relate each deformation source model to the observed displacements. The source model, $G\mathbf{m}(t)$ is:

$$\begin{aligned}G\mathbf{m}(\mathbf{t}) = &G_P P(t)_{\text{rift}} + G_S S(t)_{\text{decollement}} \\ &+ G_V V(t)_{\text{mogi}}.\end{aligned} \tag{2}$$

Additional details on the various error terms are given in Miyazaki et al. (2003) and the integration of the observation equation into the ENIF is detailed in McGuire and Segall (2003).

To model the distributed fault slip and rift opening, we subdivided the dike and decollement into a grid of rectangular patches. The ENIF only activates patches that are required to fit the data at each epoch. The edges of the dike opening were smoothed to zero using a Laplacian smoothing operator. The amount of smoothing is estimated within the ENIF from the data.

The ENIF incorporates the estimation of temporal smoothing, spatial smoothing, random walk and data error scale parameters allowing the data to determine the amount of scaling required. Previously, these scaling parameters would have been estimated using the maximum likelihood method (Segall and Matthews 1997). Temporal smoothing controls how much each estimate varies from epoch to epoch. Spatial smoothing ensures that the the stresses vary smoothly between fault patches. The random walk parameter controls how much benchmark wobble is allowed per day, and the data error scale determines how much the errors are weighted. Non-negativity constraints on fault slip and rift opening are also implemented within the ENIF (McGuire and Segall 2003).

Non-negativity constraints are imposed to keep the models physically reasonable. Rift opening, seaward decollement slip and magma chamber inflation are defined as positive. We assume that significant closing of the co-eruptive dike is not likely because it would freeze quickly at such shallow depth. Similarly, northward slip on the decollement is unlikely because it is gravity driven and the topography slopes to the south. Because we have removed the average velocities, the estimated slip and opening represent departures from steady state. We relaxed the non-negativity constraints on the magma chamber to freely allow inflation or deflation based on what the data requires.

The ENIF was run using the observation equation (Eq. 2) and daily GPS data from 1 February 1997 to 31 December 1997. The optimal dimensions of the fixed uniform opening dike were extended down to a decollement at 9 km depth. The modeled planar deformation sources were divided into patches that are 0.5 km on each side. As in the cumulative static model, we also include the summit magma chamber from Owen et al. (2000b) fixed throughout the time-dependent model at a depth of 1.2 km. The filtering results are presented in the next section.

Results

The space–time history of the best-fitting transient deformation model shows a quick acceleration of opening followed by a longer deceleration (Fig. 4). Predicted displacements from the preferred model are plotted with observed data in Fig. 3. The modeled rift opening, $P(t)_{\text{rift}}$, shows that the transient rift extension was a shallow isolated process along the rift between Nāpau and Makaopuhi craters (Fig. 5).

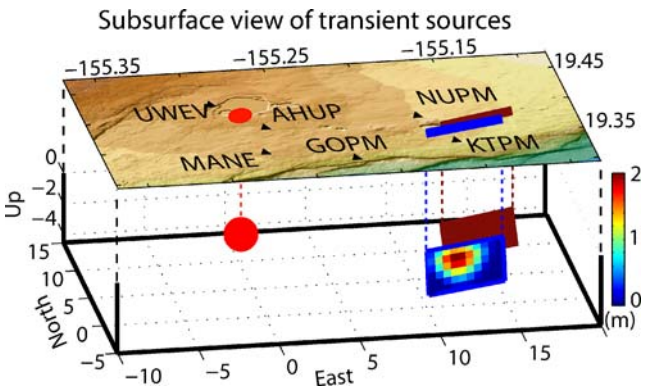

Fig. 5 Dike parallel cross section of both the 1.96 m uniformly opening 30 January 1997 intrusion dike and the cumulative distributed slip modeled in this study

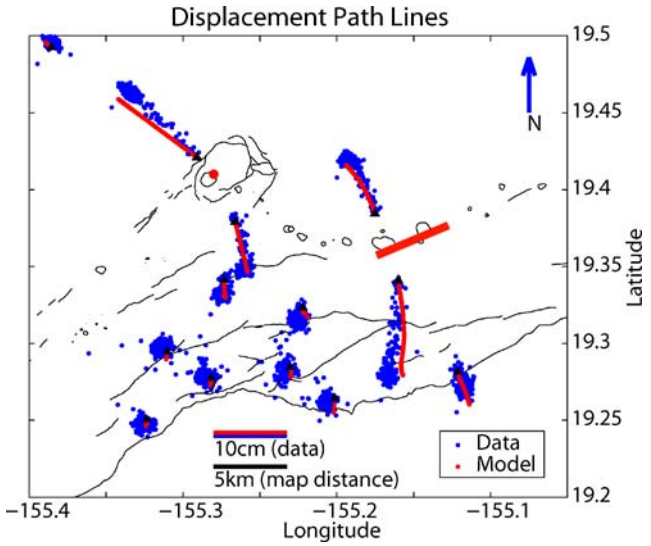

Fig. 6 Displacement pathlines of the ERZ continuous GPS stations for 290 days following the 30 January 1997 intrusion. The data are shown in *blue* and the model in *red*. The time series start at the *black triangle*

Since station velocities in this study are temporally variable, traditional maps of GPS displacement vectors limit the amount of information that can be displayed. We choose to spatially compare GPS station displacements to model-predicted displacements using discretized pathlines (see p. 367 Lai et al. 1993; Fig. 6), which show the paths traversed by GPS stations over a given time span. This is similar to pathline images of fluid flow that have been produced by long-exposure photography of floating reflectors, like micaceous mineral grains. The modeled pathlines follow the data pathlines well both temporally (Fig. 3), and spatially (Fig. 6).

To determine which model elements were required by the data, we compute weighted scalar RMS errors for three scenarios involving combinations of the summit magma chamber, rift zone, and decollement. Weighted scalar RMS errors were determined for each epoch of each model as in (Segall and Harris 1986; Fig. 7, preferred model) and then averaged over time (Table 2). Models estimating only rift opening and summit magma chamber inflation ($P(t)_{\text{rift}}$+ $V(t)_{\text{mogi}}$) were able to fit the transient data nearly as well as those including the decollement ($P(t)_{\text{rift}}$+$V(t)_{\text{mogi}}$+ $S(t)_{\text{decollement}}$). The slip on the decollement, $S(t)_{\text{decollement}}$, was negligible regardless of its depth, which was varied in

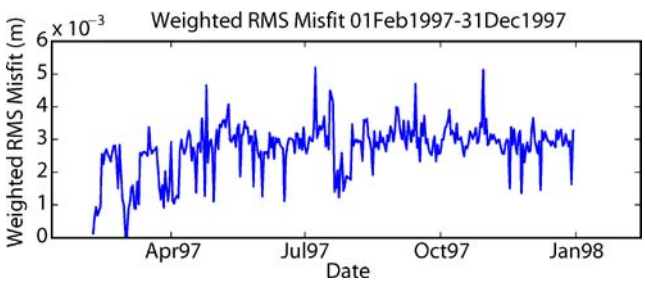

Fig. 7 Weighted RMS errors of the preferred model over time

Table 2 Model errors produced by ENIF runs using different combinations of model elements

Model	Ave. error	Max. error
$P(t)_{\text{rift}}$+ $V(t)_{\text{mogi}}$[a]	2.7 mm	5.2 mm
$P(t)_{\text{rift}}$+ $V(t)_{\text{mogi}}$+$S(t)_{\text{decol}}$	2.3 mm	5.7 mm
$V(t)_{\text{mogi}}$+$S(t)_{\text{decol}}$	Unstable	Unstable

[a]Preferred model

1-km increments from 3 to 15 km (Fig. 8). Decollement slip only slightly improved the fit to the data, so we removed it in favor of estimating fewer parameters. Models that neglected the rift and included only the decollement and summit magma chamber quickly became unstable because the model was unable to fit the data.

An alternate possibility is that the transient deformation resulted from reinflation of a shallow magma chamber beneath Makaopuhi crater, that deflated during the initial eruption (S. Owen, Personal Comm., 2004), rather than filling of a more planar rift zone body. Models with such a magma chamber recover the vertical deformation at NUPM and KTPM better than the rift only model, but overshoot the final north position of NUPM and are unable to recover the transient signal at KAEP on the coast.

To test the resolvability of large-scale features in the slip distribution using the Kalman filter, we generated three synthetic opening distributions. The first (Fig. 9a) required all of the post-intrusive opening to be between the surface and 2 km deep, on the same plane as the initial dike. The second synthetic model (Fig. 9b) opened between 2–4 km deep, and lastly we produced a model that opened completely over the whole rift zone from the surface to 8 km deep (Fig. 9c). In all cases, we are able to resolve the large-scale opening, though the exact boundaries are smoothed (Fig. 9d–f). From these examples, we are confident that the depth of opening is well resolved and the post-intrusive opening occurred below the initial dike.

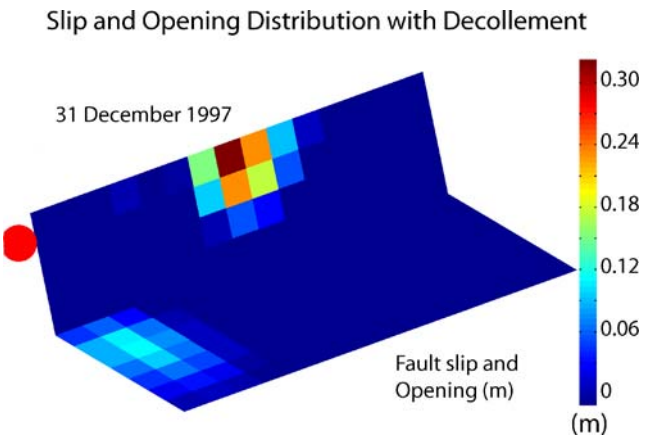

Fig. 8 Cumulative slip through 1997 in a typical model that includes a decollement at 9 km depth. Slip on the decollement was negligible on all runs where it was included, regardless of depth, so it was removed in favor of estimating fewer parameters for the preferred model

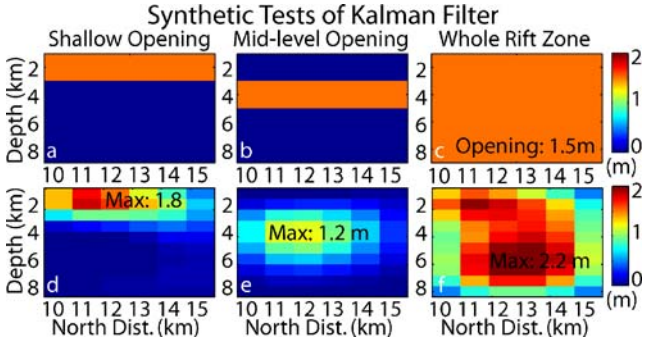

Fig. 9 Test models with opening in the top 2 km of the rift zone (**a**), opening from 2–4 km (**b**), and opening the entire rift zone (**c**). Opening distributions (**d**–**f**) show the respective estimated models corresponding to the synthetic examples

We use the opening moment rate, $\dot{M}_o(t)$, as a scalar measure of strain released in the rift zone at each epoch. Opening moment rate is defined as:

$$\dot{M}_o(t) = \mu \int \int_A \dot{P}(t)_{\text{rift}} dA \tag{3}$$

where μ is the shear modulus, A is the area that opened, and $P(t)_{\text{rift}}$ is the modeled, spatially variable, amount of opening in the rift zone as in Eq. 3.

Both rift opening rate and magma chamber inflation rate follow a similar pattern that coincides with observations of Pu'u 'Ō'ō's lava pond (Fig. 10). Rift opening accelerated for nearly 60 days until reaching its maximum rate of 7.8m/day on 3 March 1997. Rift opening then decelerated, reaching background levels by May. During the same period that the rift was dilating, the summit magma chamber was inflating. Inflation rate reached a maximum of 0.02 km^3/year a day after the rift opening rate was at its maximum. After the summit magma chamber reinflated, it stayed at a steady volume throughout the remainder of the year. The transient deformation reached its maximum rate 3–4 days after the reappearance of the lava pond at Pu'u 'Ō'ō. Deceleration of rift opening continues for several months following complete reinflation of the summit magma chamber and resumption of Pu'u 'Ō'ō's eruptions.

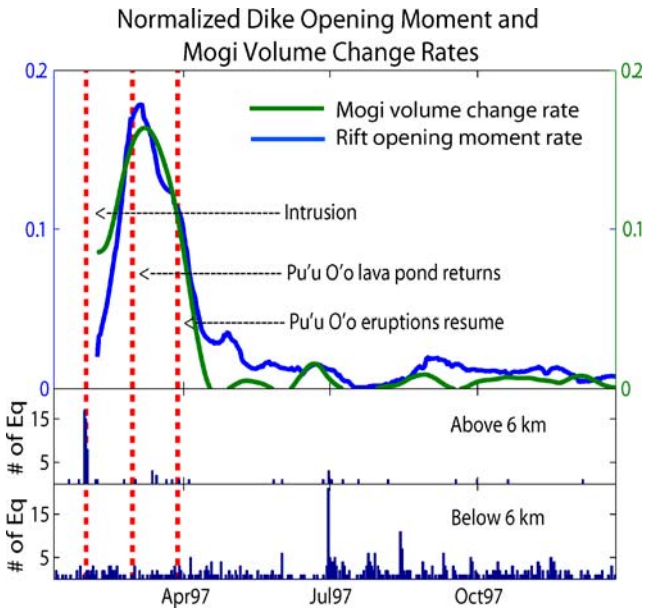

Fig. 10 Normalized time evolving of rift opening moment rate, normalized by a maximum of 7.8 m/year, and magma chamber inflation rate, normalized by a maximum volume change rate of 0.02 km^3/year. The *red dotted lines* show the time of the intrusion, the refilled lava pond at Pu'u 'Ō'ō, and the time eruptions resumed there. Both rates sharply peak just after the lava pond returns to Pu'u 'Ō'ō. *Histograms below*, are the number of earthquakes per day above 6 km in the *middle frame* and below 6 km in the *lower frame*

Discussion

We show here that the transient deformation occurred largely aseismically, but that the spatial pattern of deformation and earthquake locations are inconsistent with an elastic brittle layer overlying a viscoelastic half-space, as discussed for the Icelandic rift zones in Foulger et al. (1992).

Earthquakes on Kīlauea occur in two main clusters without an increase in either cluster throughout the transient deformation. Relocated earthquakes for the year

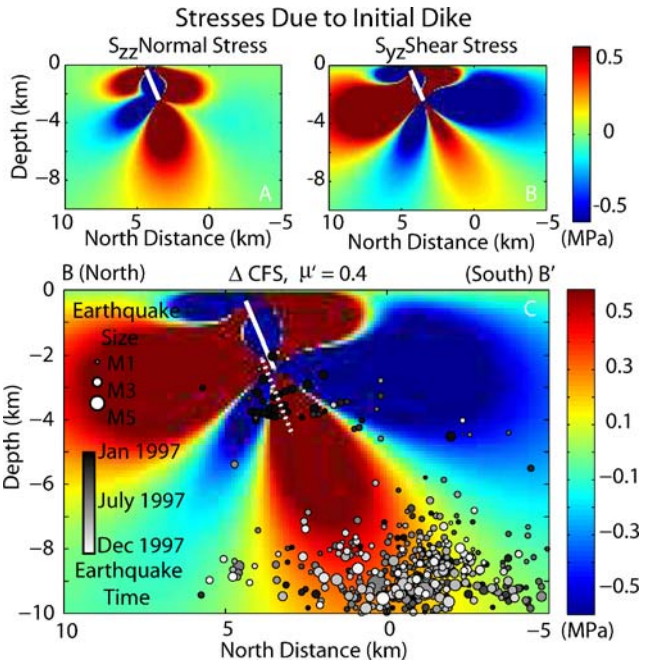

Fig. 11 Stresses due to initial dike. **a** Vertical normal stresses due to initial dike. **b** Shear stresses due to initial dike. **c** Change in Coulomb failure stress on horizontal planes due to the initial 30 January 1997 dike intrusion. *Warmer colors* are encouraged to slip by the stress change and *cooler colors* discouraged. The *white line* shows the location of the 30 January 1997 dike. Relocated south flank earthquakes are also plotted with *blacker circles* indicating earthquakes that occurred early in the year; the *whiter circles* occurred later in the year. The size of the circle indicates the magnitude of the event

of 1997 (O. Lengline, 2004, personal communication) are shown in Fig. 11, along with Coulomb stress changes which are discussed below.

One deep cluster, with earthquakes occurring between 7 to 10 km, comprises most of the south flank earthquakes. This cluster averaged 1.15 earthquakes per day throughout 1997. There was no increase in earthquake rate at these depths following the 30 January 1997 intrusion (Fig. 10).

The second cluster is shallow (2–4 km), and contains just a few events that are directly associated with the intrusion. These earthquakes occurred immediately before or during the 30 January 1997 intrusion at depths above 6 km (Fig. 10). Earthquakes immediately below an intruding dike commonly occur (Rubin et al. 1998). Two days after the intrusion, the earthquake rate returns to background levels, even though there are clear deformation signals in the GPS data, confirming that the transient deformation occurred aseismically. The absence of a change in earthquake rate on the decollement is consistent with the lack of transient decollement slip inferred from the inversion of GPS data.

We calculated the co-intrusive change in Coulomb failure stress, ΔCFS, to determine where earthquakes would be encouraged following the intrusion. We use a tension positive convention in defining ΔCFS as:

$$\Delta \mathrm{CFS} = \Delta\tau + \mu' \Delta\sigma_n, \tag{4}$$

where $\Delta\tau$ is the change in shear stress, $\Delta\sigma_n$ is the change in normal stress, and μ′ is effective coefficient of friction, which is usually between 0.0–0.75 (King et al. 1994). The stresses are calculated on horizontal surfaces that would be parallel, or nearly parallel, to the decollement (Fig. 11). We use a friction coefficient of μ'=0.4. Since the Coulomb stress change is dominated by the shear stresses (Fig. 11), the pattern of stress change does not significantly change when μ' is varied from 0.1–0.6.

The change in Coulomb stress due to the intrusion produces zones of increased stress that should coincide with increases in seismicity. The earthquakes at the depth of the decollement occur in an encouraged zone, but the ΔCFS of less than 0.35 MPa induced by the intrusion was apparently insufficient to trigger events beyond steady state rates. The shallow (<6 km) Coulomb stress change discourages slip on near-horizontal planes south of the intrusion. The shallow small cluster of earthquakes occurring in this region of negative Coulomb stress change presumably indicates that slip was not on sub-horizontal planes. The shallow flank north of the intrusion is also highly encouraged, but does not generally produce earthquakes on sub-horizontal planes, likely because of the "buttressing effect" of Mauna Loa.

Most of the earthquakes during 1997 were too small and recorded by too few stations to have reliable focal mechanisms. Got and Okubo (2003), however, determined focal mechanisms for some larger earthquakes which occurred at similar depths to the deep cluster presented here. They conclude that the dips of the focal mechanisms are in good agreement with the fault planes determined from relocations. Their example focal mechanism for a decollement earthquake (M_L 3), not to be confused with the steeply dipping reverse fault plane events they also present, show a sub-horizontal nodal plane that strikes 55°N and dips 12°N, which is consistent with near-horizontal planes for which we calculated the Coulomb stress change.

While it does not appear that any deep earthquakes were triggered by the intrusion, shallower opening at the base of the co-intrusive dike is supported by the change in rift-perpendicular normal stresses induced by the intrusion. Figure 12 shows the horizontal normal stresses induced by the intrusion. Intense horizontal normal stresses of greater than 0.8 MPa just below initial dike were high enough to cause the transient deformation at the depths of the modeled transient.

This data set does not provide sweeping generalizations about the mechanics of all rift zones, but we can discount models that require laterally extensive viscoelastic layers, as in the Icelandic model Foulger et al. (1992). The GPS data reveal deformation of the rift zone itself below the 30 January dike, but at depths less than 6 km. In addition, ongoing south flank seismicity concentrated below this depth demonstrates brittle behavior below the depths of the post intrusion transient, thus ruling out a laterally extensive viscoelastic response.

This transient rift zone deformation instead occurs on a vertical dike-like structure, rather than a horizontal layer. The same persistent pockets of magma that weakened the rift zone for the initial intrusion (Thornber et al. 2003) could have provided enough weakness along the strike to allow the transient opening.

This study shows that the time dependence of the transient deformation can be attributed to a combination of repressurization of the magmatic system and extension within the rift beneath the co-eruptive dike intrusion. We interpret the acceleration of summit reinflation and rift extension before the reappearance of the lava pond at Pu'u 'Ō'ō as the result of repressurizing the magmatic system at the same time as the rock stresses were causing

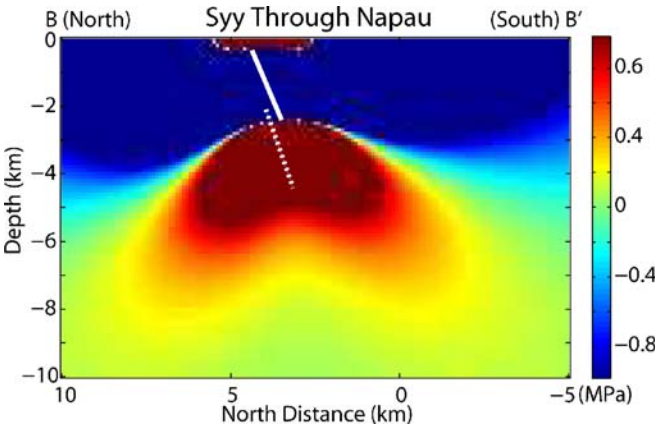

Fig. 12 Normal stresses induced by the initial 30 January 1997 dike intrusion. *Warm colors* indicate extension, *cooler colors* compression. The cross section of the resulting transient dike is shown as a *dotted line* below the initial dike cross section

the rift to continue dilating. During this period, the magmatic pressure was less than the magmastatic head at the elevation of the Pu'u 'Ō'ō vent, so the pressure continued to build. Once eruptions at Pu'u 'Ō'ō resumed, the magma pressure remained constant and equal to this magmastatic head. This is consistent with the cessation of summit magma chamber inflation just after the resumption of eruptions at Pu'u 'Ō'ō. The continued deformation following the reinitiation of Pu'u 'Ō'ō eruptions must be explained by continued accommodation of the dike, at constant magmatic pressure, due to the stresses induced by the initial intrusion.

Conclusions

The continuous GPS data on Kīlauea volcano, Hawai'i are capable of capturing not only earthquakes, intrusions and eruptions, but also transient deformation events that develop over longer timescales. The extended network inversion filter provides a framework for estimating the time-dependent source parameters causing the observed deformation. Following the 30 January 1997 intrusion, the ENIF helps us draw these conclusions:

1. Additional transient deformation of Kīlauea's ERZ occurred that resulted in up to 7 cm of additional surface displacement at sites close to the fissures
2. Cumulative displacements from 1 February 1997–31 December 1997 are well modeled as the opening of a dike-like body from 2–4.5 km deep and reinflation of the summit magma chamber
3. The opening distribution of the ENIF inversions show that the opening remains localized just below the co-eruptive dike with a maximum opening of 1.5 m
4. Temporal evolution of the model provides a time sequence of events following the intrusion:
   - 30 Jan.: Intrusion, Pu'u 'Ō'ō drains, and summit deflates
   - 30 Jan.–3 Mar.: Summit inflation and rift opening accelerate
   - 24 Feb.: Pu'u 'Ō'ō's lava pond returns
   - 3 Mar.: Summit inflation and rift zone opening begin to decelerate
   - 28 Mar.: Pu'u 'Ō'ō eruptions resume
   - 15 Apr.: Summit ceases transient inflation
   - 01 Aug.: Rift zone ceases transient opening
5. The transient deformation occurred aseismically
6. We interpret the transient deformation as resulting from the mid-crustal stress perturbation induced by the initial dike injection and repressurization of Kīlauea's magma system to an equilibrated state
7. While stresses induced by the intrusion favored slip on a decollement, we see no evidence of accelerated deformation or an increase in seismicity associated with this stress change

Acknowledgments This work was supported by the Robert and Marvel Kirby Stanford Graduate Fellowship, The Evolving Earth Foundation, and NSF Grant EAR-9902875. We would also like to thank P. Cervelli and A. Miklius for processing the GPS data, J. Murray for her help with filtering, O. Lengline for the seismic data, and S. Owen and the HVO staff for enlightening discussions.

References

Amelung F, Jónsson S, Zebker H, Segall P (2000) Widespread uplift and 'trapdoor' faulting on Galapagos volcanoes observed with radar interferometry. Nature 407(6807):993–996

Ando M (1979) The Hawaii earthquake of November 1979: low dip angle faulting due to forceful injectino of magma. J Geophys Res 84:7616–7626

Árnadóttir T, Segall P, Matthews M (1991) A fault model for the 1989 Kilauea south flank earthquake from level and seismic data. Geophys Res Lett 18(12):2217–2220

Bjórnsson A, Sæmundsson K, Einarsson P, Tryggvason E, Gronvold K (1977) Current rifting episode in north Iceland. Nature 266 (5600):318–323

Bjórnsson A, Johnsen G, Sigurdsson S, Thorbergsson G, Tryggvason E (1979) Rifting of the plate boundary in north Iceland 1975–1978. J Geophys Res 84(NB6):3029–3038

Bonaccorso A, Davis P (1993) Dislocation modelling of the 1989 dike intrusion into the flank of Mount Etna, Sicily. J Geophys Res 98(B3):4261–4268

Bonaccorso A, Aloisi M, Mattia M (2002) Dike emplacement forerunning the Etna July 2001 eruption modeled through continuous tilt and GPS data. Geophys Res Lett 29(13):1–2

Cervelli P, Segall P, Amelung F, Garbeil H, Meertens C, Owen S, Miklius A, Lisowski M (2002a) The 12 September 1999 Upper East Rift Zone dike intrusion at Kilauea Volcano, Hawaii: art. no. 2150. J Geophys Res 107(B7):2150

Cervelli P, Segall P, Johnson K, Lisowski M, Miklius A (2002b) Sudden aseismic fault slip on the south flank of Kilauea volcano. Nature 415(6875):1014–1018

Creutz M (1984) Monte-carlo study of quantized su(2) gauge theory. Phys Rev D 21:2308–2315

Delaney P, Denlinger R, Lisowski M, Miklius A, Okubo P, Okamura A, Sako M (1998) Volcanic spreading at Kilauea, 1976–1996. J Geophys Res 103(B8):18003–18023

Desmarais E, Segall P, M A (2005) A series of transient slip events on Kilauea volcano, Hawaii. EOS Trans AGU Fall Meet Suppl 85(47) G533B–G878B, Abstract

Dieterich J (1988) Growth and persistence of Hawaiian volcanic rift zones. J Geophys Res 93(B5):4258–4270

Du Y, Aydin A (1992) 3-Dimensional characteristics of dike intrusion along the northern Iceland rift from inversion of geodetic data. Tectonophysics 204(1–2):111–121

Dvorak JJ, Dzurisin D (1997) Volcano geodesy: the search for magma reservoirs and the formation of eruptive vents. Rev Geophys 35(3):343–384

Foulger G, Jahn C, Seeber G, Einarsson P, Julian B, Heki K (1992) Post-rifting stress relaxation at the divergent plate boundary in northeast Iceland. Nature 358(6386):488–490

Got J, Frechet J, Klein F (1994) Deep fault plane geometry inferred from multiplet relative relocation beneath the south flank of Kilauea. J Geophys Res 99(B8):15375–15386

Got J-L, Okubo P (2003) New insights into Kilauea's volcano dynamics brought by large scale relative relocation of microearthquakes. J Geophys Res 108(B7):2337–2350

Gregorius T (1996) GIPSY-OASIS II: how it works. Univ. of Newcastle upon Tyne, New Castle, England, UK, (self-published)

Heliker C, Sherrod D, Thornber C, Kauahikaua J (1997) Kilauea Volcano East Rift Zone eruptions update: 1997 brings era of instability. EOS Trans AGU Fall Meet Suppl 78:T21A–T28A

Hooper A, Segall P, Johnson K, Rubinstein J (2002) Reconciling seismic and geodetic models of the 1989 Kilauea south flank earthquake. Geophys Res Lett 29(22):2062–2066

Jónsson S, Zebker K, Cervelli P, Segall P, Garbeil H, Mouginis-Mark P, Rowland S (1999) A shallow-dipping dike fed the 1995 flank eruption at Fernandina volcano, Galapagos, observed by satellite radar interferometry. Geophys Res Lett 26(8):1077–1080

King G, Stein R, Lin J (1994) Static stress changes and the triggering of earthquakes. Bull Seismol Soc Am 84:935–953

Klein F (1981) A linear gradient crustal model for south Hawaii. Bull Seismol Soc Am 71(5):1503–1510

Klein F, Koyanagi Y, Nakata J, Tanigawa W (1987) The seismicity of Kilauea's magma system. US Geol Surv Prof Pap 1350:55–84

Lai W, Rubin D, Krempl E (1993) Introduction to continuum mechanics. Elsevier, Amsterdam

Larson KM, Cervelli P, Lisowski M, Miklius A, Segall P, Owen S (2001) Volcano monitoring using the Global Positioning System: filtering strategies. J Geophys Res 106(B9):19453–19464

McGuire JJ, Segall P (2003) Imaging of aseismic fault slip transients recorded by dense geodetic networks. Geophys J Int 155 (3):778–788

Metropolis N, Rosenbluth A, Rosenbluth M, Teller A, Teller E (1953) Equation of state calculations by fast computing machines. J Chem Phys 21:1087–1092

Miyazaki S, McGuire J, Segall P (2003) A transient subduction zone slip episode in southwest Japan observed by the nationwide GPS array. J Geophys Res 108(B2):2087

Mogi K (1958) Relations between the eruptions of various volcanoes and the deformations of the ground surfaces around them. Bull Earthq Res Inst Univ Tokyo 36:111–123

Nakamura K (1980) Why do long rift zones develop in Hawaiian volcanoes: a possible role of thick oceanic sediments (in Japanese). Bull Volcanol Soc Japan 25:255–267

Okada Y (1985) Surface deformation due to shear and tensile faults in a half-space. Bull Seismol Soc Am 75:1135–1154

Okada Y, Yamamoto E (1991) Dyke intrusion model for the 1989 seismovolcanic activity off Ito, central Japan. J Geophys Res 96 (B6):10361–10376

Owen S, Miklius A, Segall P, Lisowski M, Sako M (1997) Displacements from the June 30, 1997 M5.5 Kilauea south flank earthquake and preceding decrease in slip rate. EOS Trans AGU Suppl 84(46):V51E–0323

Owen S, Segall P, Lisowski M, Miklius A, Denlinger R, Sako M (2000a) Rapid deformation of Kilauea Volcano: global positioning system measurements between 1990 and 1996. J Geophys Res 105(B8):18983–18998

Owen S, Segall P, Lisowski M, Miklius A, Murray M, Bevis M, Foster J (2000b) January 30, 1997 eruptive event on Kilauea Volcano, Hawaii, as monitored by continuous GPS. Geophys Res Lett 27(17):2757–2760

Rubin AM, Gillard D, Got JL (1998) A reinterpretation of seismicity associated with the January 1983 dike intrusion at Kilauea Volcano, Hawaii. J Geophys Res 103(B5):10003–10015

Segall P, Harris R (1986) Slip deficit on the San Andreas Fault at Parkfield, California, as revealed by inversion of geodetic data. Science 233(4771):1409–1413

Segall P, Matthews M (1997) Time dependent inversion of geodetic data. J Geophys Res 102(B10):22391–22409

Segall P, Cervelli P, Owen S, Lisowski M, Miklius A (2001) Constraints on dike propagation from continuous GPS measurements. J Geophys Res 106(B9):19301–19317

Sigurdsson O (1980) Surface deformation of the Krafla fissure swarm in two rifting events. J Geophys 47(1/3):154–159

Thatcher W (1992) Does the mid-crust flow? Nature 358 (6386):454–455

Thornber C, Sherrod D, Heliker C, Kauahikaua J, Trusdell F, Lisowski M, Okubo P (1997) Kilauea's ongoing eruption: Napau crater revisited after 14 years. EOS Trans AGU Spring Meet Suppl 78:V22A–03

Thornber CR, Heliker C, Sherrod DR, Kauahikaua JP, Miklius A, Okubo PG, Trusdell FA, Budahn JR, Ridley WI, Meeker GP (2003) Kilauea east rift zone magmatism: an Episode 54 perspective. J Petrol 44(9):1525–1559

Thurber C, Gripp A (1988) Flexure and seismicity beneath the south flank of Kilauea Volcano and tectonic implications. J Geophys Res 93(B5):4271–4278

Walker G (1987) The dike complex of Koolau Volcano, Oahu: internal structure of a Hawaiian rift zone. US Geol Surv Prof Pap 1350:933–961

Walpersdorf A, Vigny C, Ruegg JC, Huchon P, Asfaw LM, Kirbash SA (1999) 5 years of GPS observations of the Afar triple junction area. J Geodyn 28(2–3):225–236

Wyss M (1988) A proposed source model for the great Kau, Hawaii, earthquake of 1868. Bull Seismol Soc Am 78:1450–1462

Zumberge JF, Heflin MB, Jefferson DC, Watkins MM, Webb FH (1997) Precise point positioning for the efficient and robust analysis of GPS data from large networks. J Geophys Res 102 (B3):5005–5017